LA-UR 90-4370

Received by OST

JAN 0 8 1991

LA-UR--90-4370

DE91 005946



TITLE: Unifying the Controlling Mechanisms for the Critical Heat Flux and Quenching: The Ability of Liquid to Contact the Hot Surface

AUTHOR(S): Cetin Unal, Vincent Daw, and Ralph Nelson

SUBMITTED TO: 1991 ASME/AIChE National Heat Transfer Conference
July 28-31, 1991
Minneapolis, Minnesota

## DISCLAIMER



Los Alamos Los Alamos National Laboratory
Los Alamos, New Mexico 87545

FORM NO 836 R4
ST NO 2629 5/81

# Unifying The Controlling Mechanisms for the Critical Heat Flux and Quenching: The Ability of Liquid to Contact the Hot Surface

by

Cetin Unal, Vincent Daw, Ralph A. Nelson

Los Alamos National Laboratory
Nuclear Technology and Engineering Division
Engineering and Safety Analysis Group
Los Alamos, NM 87545

## ABSTRACT

We investigate the hypothesis that the critical heat flux (CHF) occurs when some point on a heated surface reaches a temperature high enough so that liquid can no longer maintain contact at that point, resulting in a gradual but continuous increase in the overall surface temperature. This hypothesis unifies the occurrence of the CHF with the quenching of hot surfaces by relating them to the same concept: the ability of a liquid to contact a hot surface, generally defined as some fraction of liquid's homogeneous nucleation temperature, depending upon the contact angle.

The proposed hypothesis about the occurrence of the CHF is investigated through study of the boiling mechanism of the second transition region of nucleate pool boiling. A two-dimensional transient conduction heat-transfer model was developed to investigate the heat-transfer mechanism. The initial macrolayer thickness on the dry portion of the heater, in the second transition region, was found to be bounded between 0 and 11 microns for a copper heater. The radius of the dry patch varied from 15 to 23 mm (60% and 92% of the heater radius, respectively) for initial macrolayer thicknesses of 0 and 11 microns, respectively.

The results indicated that the critical liquid-solid contact temperature at the onset of CHF (the surface temperature at the center of the dry patch) must be lower than the homogeneous nucleation temperature of the liquid for the pool boiling of water on a clean horizontal surface. The liquid-solid contact temperature was dependent upon the initial liquid macrolayer thickness, varying from 180°C to 157°C for initial macrolayer thicknesses of 0 and 11 microns, respectively. These values are in good agreement with extrapolated contact temperature data at the onset of film

boiling. This indicates that the mechanism for the occurrence of the CHF could be similar to the mechanism generally accepted for the quenching of the hot surfaces.

Further study of this mechanism to better understand observed trends in other experimental results shows qualitative agreement with those results. These include a significant decrease in the radius of the dry patch to 4 mm (16% of the heater radius) when the thermal conductivity of the heater was decreased to that corresponding to nickel. When the thickness of a copper heater was decreased from 10 mm (representing an infinitely thick medium) to 0.1 mm, a dry patch radius of 2.25 mm (9% of the heater radius) was found to be sufficient for the temperature at the center of the dry patch to reach the critical contact temperature. These comparisons are felt to provide some understanding as to why the second transition region has been observed only in limited cases.

## Nomenclature

| | |
|---|---|
| $c$ | Specific heat capacity |
| $h$ | Heat-transfer coefficient |
| $H$ | Heater thickness |
| $k$ | Thermal conductivity |
| $LP$ | Integer defining the heat flux boundary condition |
| $N/A$ | Nucleation site density |
| $r$ | Space coordinate |
| $Q_o$ | Heat generation |
| $q$ | Heat flux |
| $t$ | Time |
| $T$ | Temperature |
| $z$ | Space coordinate |
| $\Delta T_{BL}$ | Wall superheat at the bottom-left corner of the heater (see Fig. 3-b) |
| $\Delta T_{BR}$ | Wall superheat at the bottom-right corner of the heater (see Fig. 3-b) |
| $\Delta T_{TL}$ | Wall superheat at the top-left corner of the heater (see Fig. 3-b) |
| $\Delta T_{TR}$ | Wall superheat at the top-right corner of the heater (see Fig. 3-b) |
| $\beta_a$ | Advancing contact angle |
| $\delta$ | Macrolayer thickness |
| $\Delta$ | $T - T_{sat}$ |
| $\rho$ | Density |
| $\tau$ | The lifetime of the vapor mushroom (hovering period) |

| | |
|---|---|
| $n\tau$ | The number of hovering periods |
| $< >$ | Time dependent, surface-averaged |

## Subscripts

| | |
|---|---|
| av | surface-time average |
| CHF | critical heat flux |
| d | dry patch |
| h | heater |
| hn | homogeneous nucleation |
| rew | rewetting |
| s | stem |
| sat | saturation |
| 1 | dry patch region |
| 2 | two-phase macrolayer region |

## I. Introduction

Of the three boiling heat-transfer regimes (nucleate, transition, and film boiling), nucleate boiling is the regime most important for industrial applications. Although this has resulted in the study of nucleate boiling phenomena for at least three decades, prediction still remains principally an empirical art. The nucleate boiling region on a classical boiling curve of heat flux versus wall superheat (q vs $\Delta T_{sat}$) starts with incipient boiling and extends until the first boiling crisis, critical heat flux (CHF). The heat transport mechanisms between incipient boiling and the CHF point change considerably. Typical regions classified by Gaertner[1] from his experimental study are a) incipient boiling, b) discrete bubble region, c) first transition region, d) vapor mushroom region, e) second transition region, and f) CHF. The pool nucleate boiling portion of the boiling curve obtained by Gaertner for a polished copper surface is shown in Fig. 1, and sketches of the boiling phenomena are shown in Fig. 2.

Of these subregions within nucleate boiling, the CHF point has been given a significant amount of study. Studies of the CHF phenomena mainly fall into three categories:[2] empirical correlations, bubble interaction models, and hydrodynamic instability models. For the empirical models,[3,4,5] the CHF is expressed in terms of dimensionless groups, and either a statistical fit or a fit based upon some simple model is obtained. Bubble interaction models[6,7] consider the CHF to be limited by the removal rate of bubbles, which carry away the heat in the form of evaporation. This theory was based on critical bubble spacing near the heated surface. The hydrodynamic model, based on the instability of a wave at the liquid/vapor interface, was first proposed by Chang,[8] but was completed by Zuber.[9,10,11] This approach assumes that near the CHF point the heating surface is covered by rising vapor columns

in the form of vapor jets, with countercurrent liquid jets flowing downward to replenish the evaporation loss. When the relative velocity is high enough, an instability (Kelvin-Helmholtz) occurs and the vapor jets collapse. This collapse produces the CHF condition by preventing the escape of the vapor, and since the surface is vapor covered, by preventing the return of liquid to the surface. Although Zuber's instability theory is significant and superior to the others, it neither explains nor predicts the experimental data obtained for finite flat plates of various sizes, geometries, and surface conditions.

The most important experimental observation to challenge Zuber's hydrodynamic theory was the detection of a thin liquid macrolayer with many vapor stems on the heated surface.[12,13] Haramura and Katto[14] postulated that CHF will occur if the heat flux is high enough to evaporate the macrolayer prior to departure of the vapor mushroom bubble. This picture, then, is for a macrolayer *uniformly* distributed over the heater surface. This model does not contradict Zuber's hydrodynamic instability model, but instead extends the physics for a more complete description of the phenomenon. One may consider this theory to be a fourth category of CHF modeling and call it a surface-controlled theory. A surface-controlled theory postulates that the CHF occurs when a thin layer of liquid that is assumed to exist between the vapor mass and the heater surface completely evaporates before the vapor mass leaves the surface, as suggested first by Katto and his coworkers. Katto's multistep CHF model considers steady-state conditions. Pasamehmetoglu and Gunnerson[15] showed that it can be extended to explain transient CHF phenomena.

None of the models we have discussed above consider the dry patches observed by Gaertner[1] in the second transition region leading up to the CHF point. It is important to note that it is the much poorer heat transfer provided by the dry patches, as opposed to

the macrolayer-covered surface, which is believed to create the change in slope of the boiling curve at this point (see Fig. 1). Kirby and Westwater[12] and Van Ouwerkerk[16] also indicated that dry spots sometimes appear in the liquid film at high heat fluxes near the CHF point. In fact the occurrence of dry patches and patchwise boiling has been previously observed by Corty and Foust,[17] Carne,[18] and Torikai.[19] A detailed summary of findings from these studies regarding dry patch formation is given in the following section.

As the time- and area-averaged surface temperature represented on the boiling curve in the second transition region increases, the number and size of the patches increases.[12,16] Vapor mushrooms still exist above the heater surface and are still responsible for the transport of vapor from the surface. During the life of a mushroom bubble prior to its departure from the surface, these dry spots appear and grow in size. After bubble departure, liquid washes across the dry area and rewets the surface. This transient process of bubble growth and departure is repeated over and over for any give point on the boiling curve and produces the "steady-state" data represented by the boiling curve. It seems obvious that local-instantaneous surface temperatures within these dry patches will increase as a function of time and position as the patch grows.

As the heat flux increases to higher levels on the boiling curve, the local-instantaneous surface temperatures within the dry patches will eventually increase to a point where rewetting of the surface is no longer possible. Although it has been indicated by several researchers that these dry patches are important to the understanding of the boiling crisis, it has not received much attention due to both experimental difficulties in determining dry patch behavior and computational difficulties in solving any model constructed to address the phenomena. We believe

these dry patches provide the key to understanding the mechanism which produces the CHF.

The thickness of the liquid macrolayer must vary from one point to another on the heater surface and show some statistical distribution. We believe that the formation of the dry patches is a result of the evaporation of the thinner regions of the local liquid macrolayer. This might be considered a simple extension of Katto's CHF theory, which assumes a uniform macrolayer thickness. However, it is not the evaporation of the liquid macrolayer and the corresponding occurrence of these dry patches themselves that causes CHF. The temperature at the center of the dry patch must first reach some critical value above which liquid-solid contact is no longer possible. Once this condition occurs at a local point on the heater surface, the hot spot begins to grow until the dry patch finally covers the entire heater surface.

Conceptually, this is very exciting because it unifies the occurrence of the CHF with the quenching of hot surfaces by relating them both to the same governing mechanism, i.e., the ability of liquid to contact a hot surface, generally defined in terms of the liquid's homogeneous nucleation temperature. While quenching of hot surfaces (the second boiling crisis) will not be discussed here, it is generally accepted that quenching is controlled by this process.[20,21] Recently, Ramilison and Lienhard[22] indicated that the liquid-solid contact temperature at the onset of the film boiling is contact-angle dependent: it approaches the homogeneous nucleation temperature of the fluid when the contact angle goes to zero (highly wetting fluids) and decreases with increasing contact angle.

This paper investigates the validity of the above hypothesis that the CHF is controlled by the occurrence of a hot spot on a heated surface where (on a transient-local basis)

the critical rewetting temperature (related to the homogeneous nucleation temperature of the liquid) is reached. The modeling approach for the heat-transfer mechanism in the second transition region was based upon a transient microscopic (nonaveraged) approach to the phenomena in this particular regime.

## II. Background on the Size and Formation of Dry Patches

While we arrived at the idea of a hot-spot-controlled CHF independently, we soon found that it had, in fact, been advanced previously by others. Research in the area of "hot spot" or "dry patch" CHF has involved work in three main areas: 1) thin horizontal boiling surfaces— size, formation, and growth of dry patches investigated but no work done on the contact temperature; 2) thick horizontal boiling surfaces— formation of dry patches observed; 3) wires— spatial distribution of dry patches along the length of a wire, with much "CHF hot spot temperature" work done. Dry patch formation on horizontal flat boiling surfaces and horizontal wires could show slightly different characteristics due to the hydrodynamics of vapor mushroom. In this paper, emphasis is given to the formation of dry patches on horizontal flat boiling surfaces. Therefore, the following subsections will discuss the first two of these three areas in more detail. Detailed information regarding wires is available in Ref. 23.

### A. Thin Horizontal Surfaces

Kirby and Westwater[12] conducted pool boiling experiments with carbon tetrachloride and methanol on a horizontal glass surface plated with an extremely thin conducting material. Near the CHF, they observed irregular vapor masses, rather than individual bubbles, hovering above a thin liquid layer. A sketch of the vapor masses observed in this study is shown in Fig. 2-a. Their description of the vapor masses was similar to

that of Gaertner. Under these vapor masses, a bubble would nucleate at a site, expand into the vapor mass, then suddenly burst, leaving only a small wake as a clue to its disappearance. As illustrated in Fig. 2-a, irregular vapor masses were sometimes followed immediately by the appearance of a dry spot on the heater surface (dark spots). These dry spots were measured to be as large as 1.8 mm in diameter and sometimes grew to merge with neighboring ones as indicted in Fig. 2-a.

The importance of Kirby and Westwater's observation is in the irregular nature of the vapor masses which lie above the thin liquid film. Previously, several researchers postulated that individual bubbles lie above a thin liquid layer (microlayer), and that the growth of a bubble was due to evaporation of this thin liquid microlayer. Kirby and Westwater, however, indicated that evaporation of the liquid film results in the growth of large, irregular vapor masses. They postulated that sizable dry spots may develop under the large vapor masses if the liquid layer completely evaporated, whereas only small dry spots can develop under bubbles, which are comparatively small. The typical lifetime of a dry spot was measured to be 10 ms, after which liquid again washed across the area and wet the solid. Since Kirby and Westwater's heater had almost no thermal mass, the rapid growth of the dry areas could result in the CHF.

Van Ouwerkerk[16] experimentally studied the occurrence of dry areas using n-Heptane on a 20-mm-thick, round Pyrex plate with a diameter of 0.2 m. The plate was heated by passing an electric current through a transparent electroconductive layer (gold sandwiched between two layers of bismuth oxide), which was deposited on the plate. Van Ouwerkerk reported a vapor structure similar to that described by Kirby and Westwater: a thin layer of liquid lying under a vapor mass. New bubbles nucleate and coalesce in this liquid layer. Dry spots occurred under each of these bubbles under the large vapor mass. Evaporation of the liquid film caused these dry spots to grow

and to merge with neighboring ones to form larger dry areas. In the next hovering period, the solid was normally wetted when liquid rushed to the surface. If the heat flux was sufficiently high, at some point on the heated surface a dry area was not wetted and started growing, leading to burnout. Van Ouwerkerk also observed that the formation and disappearance of dry areas continued at other points while the critical one continued to grow. It is interesting to note that at atmospheric pressures the dry areas formed a square grid at 10-mm intervals. The maximum size and lifetime of dry areas did not change significantly when the heat flux varied from 80% to 100% of the burnout value. The frequency of their occurrence, however, did increase with increasing heat flux.

### B. Thick Horizontal Surfaces

One of the earliest papers reporting information on patchwise boiling using organic fluids was published by Corty and Foust.[17] They observed that stable patchwise boiling on a thick, rectangular horizontal copper plate was possible. The wall superheats in these liquid patches were at typical nucleate boiling values while the bare spots were at much higher superheats.

Carne[18] studied pool boiling of organic fluids and water at atmospheric pressures on horizontal steel elements with various diameters. He visually observed that a small vapor patch instantaneously occurred at some random location on the heater surface. He postulated that the fluid local to the patch passes through a transition boiling state where the mode of heat transfer changes from nucleate to film boiling. The occurrence of the local transition boiling was thought to be due to the local vapor flow rate causing hydrodynamic instability in the boundary layer.

The existence of an unexpected region beyond the vapor mushroom region was first reported by Gaertner[24] when he studied the nucleation characteristics of nickel salt solution on a thick horizontal copper block 50 mm in diameter. The boiling curve indicated that the heat-transfer coefficient was decreased when the heat flux was above 317,000 Btu/(hr·ft$^2$). Gaertner postulated that the occurrence of the second transition region was due to either the unique properties of the nickel salt solution or geometry, orientation, and heater surface effects. Finally, he stated that at high heat fluxes, the formation of dry patches large in comparison to individual bubbles could be responsible for the decrease in heat-transfer rate.

Later, in 1965,[1] Gaertner repeated this experiment for water with similar-sized heaters made of copper and platinum. The second transition region was again observed. In this region, he thought that the stems of the vapor mushrooms became hydrodynamically unstable at the local surface areas which had a critical active-site population. The collapse of vapor stems thus forms a local vapor patch on the heater surface. In the same paper, Hsu questioned this hypothesis and pointed out that the predicted critical wavelength for the water-stem system was much greater than the height of the stems under the vapor mushroom. Gaertner's answer to this comment was not clear and he indicated that more experimental data was needed.

Gaertner also speculated that the reason these vapor patches were not seen on small wires, thin strips, and small tubes was that the heat capacity for these heaters is small. It was also difficult to distinguish vapor patches from a vapor mushroom on the horizontal copper plate. Thus, no information on the size and the formation of these vapor patches was reported. The sketch shown in Fig. 1 (similar to that given by Gaertner) for the vapor structure in the second transition region implies that a significant amount of the surface area can be covered by vapor patches. This sketch

also implies that the patch appears over only part of the heater surface. An imagined top view of the heater is illustrated in Fig. 2-b. As shown in the figure, the patches can occur in different sizes at several different locations on the heater surface. The locations of these patches could be stationary or nonstationary for each bubble cycle (hovering period). More definite information on this is not currently available.

## III. The Heat-Transfer Model for the Second Transition Region of Nucleate Boiling

Boiling systems are frequently modeled using one of the following two approaches:

1) Microscopic. Transient phenomena for individual boiling regimes are considered.

2) Macroscopic. Quasi-steady transient responses are considered and the entire boiling curve is considered and defined through a system of empirical or phenomenologically based correlations. This approach is usually done using time- and area-averaged results, a fact which is usually not stated explicitly.

The approach taken in this research is to study the boiling phenomena in the vicinity of the boiling crisis on a microscopic, transient level.

The term "steady-state," as used in boiling heat transfer, really means that the total time over which process averaging is done is large enough to include a sufficient number of periods of the controlling phenomena to produce a time-averaged quantity that is constant from one time window to the next; i.e., the quantities typically used to represent the process are stationary. Heat flux (energy transferred to the fluid from the

surface per unit area and time) and surface temperature are such quantities. If one were to consider the steady-state process in terms of a time period shorter than that which produces stationary quantities, it would become apparent that the controlling physical phenomena involved in the boiling process are really transient, even in a "steady-state" situation. The steady-state data available in the literature allow us to develop detailed, microscopic transient physical models of the boiling process. This is done by making time and space averages of calculated quantities to compare to data. We have applied this approach in our study of the second transition region of nucleate boiling.

The key to the development of a dry patch model in the second transition region is the solution of the transient two-dimensional conduction problem in a heater under various boundary conditions (see Fig. 3-a). This problem is solved in a manner similar to the method used by Pasamehmetoglu and Nelson.[25] The wetted portion of the heater, denoted as a two-phase macrolayer region, includes the macrolayer with numerous vapor stems. The rate of heat transfer from this region is represented by a surface-averaged, time-dependent heat-transfer coefficient, $h_2$. The major difficulty in developing the model is the construction of a realistic representation of the "dry" portion of the surface. Remember that this portion is actually dry only for some fraction of the lifetime of the vapor bubble. A realistic estimate of when during the vapor mushroom's lifetime a dry patch appears and how it appears and grows must be made. During the time that dry patches occur, the rate of heat transfer from the dry portion of the heater is represented by a surface-averaged, time-dependent heat-transfer coefficient, $h_1$. The determination of $h_1$ and $h_2$ will be discussed in greater detail in sections III.A and III.B.

For the dry patch model shown in Fig. 3-a, the two-dimensional heat conduction equation in cylindrical coordinates is given for the heater by

$$\rho_h c_h \frac{\partial T}{\partial t} = k_h\left(\frac{\partial^2 T}{\partial r^2} + \frac{1}{r}\frac{\partial T}{\partial r} + \frac{\partial^2 T}{\partial z^2}\right) + LP \times Q_0 \quad , \qquad (1)$$

where LP is an integer quantity representing the problem type and is equal to 1 for internal heat generation and 0 for the boundary condition of constant heat flux or temperature at the lower end of the heater. In this study, the constant heat flux boundary condition at the bottom of the heater is used for all calculations except for the thin copper heater, where the internal heat generation option was used.

Symmetrical radial boundary conditions are used at r=0 and $r=r_h$ for all z. Thus, the radial temperature gradient becomes zero at those boundaries:

$$\frac{\partial T}{\partial r} = 0 \quad . \qquad (2)$$

At z=0 for all r, the heat flux is specified as the surface- and time-averaged (STA) experimental heat flux if a thick heater is considered (in this case, this is the CHF value):

$$-k_h \frac{\partial T}{\partial z}\Big|_{z=0} = q_{CHF} \quad \text{for LP=0} \quad . \qquad (3)$$

For thin heaters, the internal heat generation option, LP=1, is used. In this case, the bottom of the heater is considered to be perfectly insulated.

$$\frac{\partial T}{\partial z}\Big|_{z=0} = 0 \quad \text{for} \quad LP=1 \quad . \qquad (4)$$

At z=H, the boundary conditions are the surface-averaged, time-dependent heat-transfer coefficients for both the dry patch and macrolayer regions, and are given by

$$-k_h \frac{\partial T}{\partial z}\Big|_{z=H} = \langle h_1 \rangle \, (T(H,r,t)-T_{sat}) \quad \text{for} \quad 0 < r < r_d \,, \tag{5}$$

where

$$\langle h_1 \rangle = \begin{cases} \langle h_1 \rangle(t) & \text{for} \quad 0 < t < t_d \\ 0 & \text{for} \quad t_d < t < \tau \end{cases} \tag{6}$$

and

$$-k_h \frac{\partial T}{\partial z}\Big|_{z=H} = \langle h_2 \rangle \, (T(H,r,t)-T_{sat}) \quad \text{for} \quad r_d \le r \le r_h \quad \text{and} \quad 0 < t < \tau \,. \tag{7}$$

Determination of $\langle h_2 \rangle$ and $\langle h_1 \rangle$ are discussed in sections III.A and III.B, respectively. Note that while the spatial averaging brackets, < >, are shown in Eqs. 5 through 7, they will be dropped for convenience in the remainder of the paper.

After the vapor mushroom departs, the model assumes that fresh saturated liquid wets the surface. The surface temperatures in both dry patch and macrolayer regions at the time of rewet are calculated through the instantaneous contact temperature relationship.[25]

The initial temperature distribution in the heater for the problem described above is obtained in two steps. In the first step, a single-vapor-stem calculation is performed using Pasamehmetoglu and Nelson's[25] solution method. A sketch of the model used for the stem calculation is shown in Fig. 3-b. It should be noted that the stem calculation considers only a single vapor-stem/macrolayer configuration, representing the heat transfer from the whole heater surface through an average vapor stem. It involves relatively small dimensions (on the order of several hundreds of microns)

relative to the dimensions of the dry patch model (on the order of centimeters). The first step calculates the time-dependent, surface-averaged heat-transfer coefficient, $h_2$, as well as the instantaneous heater temperature distributions within the heater and macrolayer for the hovering period in which convergence to a stationary solution is obtained. In the second step, the time-dependent heat-transfer coefficient $h_2$ and the heater temperature distribution at the end of the convergent hovering period obtained from the first step are used as the boundary and initial conditions for the large-diameter heater shown in Fig. 3-a. No dry region was assumed, so that $h_2$ was assigned to the whole upper surface of the heater. The governing equation for the heater was solved numerically for several hovering periods until convergence between calculated parameters in two consecutive hovering periods was obtained. Finally, the calculated heater temperature distribution (a function of z only) at the end of the converged hovering period was assumed to exist and was used to define the initial temperature conditions within the heater for the general problem formulation of the heat-transfer characteristics in the second transition region.

The governing equations were solved using an explicit finite-difference scheme. With small time steps, the explicit finite-difference solution yields accurate results. The experimental wall heat flux was used as a lower (z=0) boundary condition and the size of the dry patch was input into the model. The size of the dry patch was varied until the predicted STA wall heat flux agreed with the input at the lower boundary.

In the case of the relatively large dry patches, which might have been the case in Gaertner's experiment, the initial temperature distribution in the heater for each succeeding hovering period would change. Thus, the governing equations had to be solved for several hovering periods. The dry patch boundary, $r_d$, for this calculation then represents the "average boundary." The calculation is started from an initial

temperature distribution as explained above. As in the single-stem/macrolayer calculation, the instantaneous temperature distribution of the last time step of the previous hovering period becomes the initial heater temperature distribution for the next hovering period. The transient calculation was terminated when the convergence criteria was satisfied, i.e., when the STA wall heat flux and temperature between two consecutive hovering periods are unchanged. If the STA (over the last hovering period) wall temperature and heat flux do not agree with the measured value (lower boundary input value), the size of the dry patch is varied and the calculation is restarted. This procedure is repeated until agreement between the calculated and measured information is achieved.

The following subsections will present the details of the calculation of $h_2$ and $h_1$.

## A. Calculation of the Surface-Averaged, Time-Dependent Heat-Transfer Coefficient, $h_2$, Representing the Macrolayer Region (Wetted Region)

The two-phase macrolayer region, shown in Fig. 3-a, is characterized by numerous vapor stems and a liquid macrolayer. Figure 3-b shows the modeled geometry of a single stem. The evaporation of the liquid macrolayer is the main mechanism for transporting energy from the heater to the vapor mass. This process is very efficient; thus, the STA wall superheat in the macrolayer region is expected to be lower than the measured STA wall superheat in the second transition region. At the CHF, the STA wall superheat for the macrolayer region can be estimated by the wall-heat-flux/wall-superheat relationship suggested by Gaertner[1] for the vapor mushroom region, as shown in Fig. 1 (point A). At point A, the STA wall superheat is 20.3°C while the measured STA wall superheat, which is really the CHF, is 43.4°C. The overall heat transfer in the wetted region is represented by a time-dependent, surface-averaged

heat-transfer coefficient, $h_2$, that is used in the proposed model. This coefficient can be obtained from the model and method developed by Pasamehmetoglu and Nelson[25] valid at point A of Fig. 1.

To obtain $h_2$, a stem calculation was performed for a copper heater representing Gaertner's heater. Calculations have shown that a 10-mm thickness can be used to represent an infinitely thick copper block. The STA wall heat flux and the number of conduction nodes in the heater and liquid macrolayer were input parameters. The stem and other calculations presented in this paper were performed for a CHF of 1.554 $MW/m^2$, the value reported by Gaertner. Details of the input parameters defining the finite-difference node sizes and the calculated output parameters for the stem calculation are available in Ref. 23.

The surface-averaged, time-dependent heat-transfer coefficient, $h_2$, representing the transient heat transfer in the macrolayer region, was calculated by dividing the calculated instantaneous surface-averaged wall heat flux by the calculated instantaneous surface-averaged wall superheats. The result is shown in Fig. 4 with the symbol 1. The heat-transfer coefficient $h_2$ is relatively high at the beginning of the new hovering period. This is because when fresh saturated liquid wets the surface, the surface temperature, calculated through the instantaneous contact temperature relations, decreases. Conduction within the heater then transports significant energy early in the bubble's lifetime to reheat the surface. The increase in the surface heat flux and a decrease in wall temperature result in a small but significant increase in $h_2$. Later, in the window between 5% and 90% of the hovering period, $h_2$ gradually increases. At the end of the hovering period, the heat-transfer coefficient increases at a relatively faster rate. In this period, the liquid macrolayer thickness becomes relatively thin, causing the conduction through the liquid macrolayer to increase

significantly. This increases the surface-averaged heat-transfer coefficient as shown in Fig. 4. The surface-averaged, time-dependent heat-transfer coefficient $h_2$ is calculated in the same manner for both the 10-mm-thick nickel and 0.1-mm-thick copper heaters.

## B. Calculation of the Surface-Averaged, Time-Dependent Heat-Transfer Coefficient, $h_1$, Representing the Dry Patch Region

The determination of the surface-averaged, time-dependent heat-transfer coefficient for the dry region, $h_1$, uses the same approach and model used in determining $h_2$. The only difference is in the specification of the initial liquid macrolayer thickness and the initial heater temperature distribution. With a specified initial macrolayer thickness and heater temperature distribution, the governing equations are solved only for a time period, $t_d$, necessary to completely evaporate the macrolayer.

The initial heater temperature distribution is specified based upon the temperature of the heater prior to the occurrence of a dry patch at a location on the heater surface; this particular location experiences a boiling process seen in the vapor mushroom region of nucleate boiling. Thus, the initial heater temperature can be obtained by performing a stem calculation as explained above in section III.

The difficult part is the selection of the initial macrolayer thickness that will dry out and cause the dry patch. Several different alternatives were tried in order to realistically estimate this thickness. In the first approach, we asked the question "what initial macrolayer thickness would evaporate in a hovering period at the heat flux level (0.906 $MW/m^2$) corresponding to the beginning of the second transition region?" The answer to this question can be obtained by conducting a stem calculation with an initially guessed macrolayer thickness at a heat flux of 0.906 $MW/m^2$. The initial

macrolayer thickness that would evaporate in a hovering period (73 ms at 0.906 $MW/m^2$) was found to be 35 microns. This value represents an upper limit for the surface-averaged initial macrolayer thickness that might exist on the part of the heater where the dry patches occur. It is an upper bound because the Helmholtz instability would decrease the thickness at higher heat fluxes. It was assumed that an initial macrolayer thickness of 35 microns existed on the heater surface where a dry patch occurred at each heat flux level in the second transition region, including the CHF.

We also chose two other initial thicknesses for the macrolayer in the evaluation of $h_1$, 11 and 8 microns. The initial thickness of 11 microns was selected based upon Haramura's recent study.[26] He obtained transient surface-averaged heat flux measurements with simultaneously taken high-speed photographs on a constant-temperature surface (horizontal tube) heated by electric current. He postulated that the heated surface begins to dry when the heat flux begins to decrease while a coalesced bubble covers the surface. Therefore, heat added in the interval between the time when the coalesced bubbles are formed and the time when the heat flux begins to decrease might equal the latent heat of the liquid layer. Using this argument, he calculated an 11-micron initial macrolayer thickness for a stainless steel rod heater 0.69 mm in diameter. As it will be shown, this thickness also represents an upper limit since it was calculated using a surface-averaged heat flux. The third value of 8 microns is simply an intermediate value. Thus we can say that the initial minimum macrolayer thickness occurring in the dry patch region could theoretically vary between 0 and 35 microns.

The time required to evaporate the macrolayer (drying time), $t_d$, can be estimated from a heat-balance equation using STA heat flux. The drying times were estimated to be 47.7, 14.99, and 10.9 ms for initial thicknesses of 35, 11, and 8 microns at an STA heat

flux of 1.554 MW/m$^2$. Due to the explicit nature of the finite-difference solution, the numerical solution was not stable when the macrolayer thickness was close to a value corresponding to the two axial node sizes in the macrolayer. (This is simply a result of our current numerics and has no real physical or numerical meaning.) Therefore, care was taken to prevent this numerical instability by increasing the number of axial nodes in the macrolayer and assuming that the macrolayer was completely evaporated when the thickness of the macrolayer calculated at the last time step was less than 1.5 microns. This mandated an adjustment of the drying times, and they were found to be 47.3, 15.15, 10.57 ms for initial thicknesses of 35, 11, and 8 microns, respectively. The ratio of the initial thickness to the number of nodes in the macrolayer was kept constant for all runs determining $h_1$.

The calculated instantaneous heat-transfer coefficients $h_1$ for initial thicknesses of 35, 11, and 8 microns are given in Fig. 4 for a 10-mm-thick copper heater. As the initial thickness decreases the instantaneous heat-transfer coefficient increases.

## IV. Results and Discussion

This section discusses several aspects of the dry patch second transition region problem. First, the necessary surface dry patch areas corresponding to different drying times are determined if homogeneous nucleation is used as the criteria for liquid-solid contact at the center of the dry patch. Second, the bounds on the initial dry patch macrolayer thickness are refined. Third, an improved estimate of the critical liquid-solid contact temperature is made and compared to available data. And finally, the effects of heater material and thickness on dry patch size are studied.

## A. Surface Areas and Drying Times Required for the Temperature at the Center of the Dry Patch to Reach the Homogeneous Nucleation Temperature of the Fluid

The homogeneous nucleation temperature of water at atmospheric pressure was calculated by the equation suggested by Lienhard[27] to be 345°C. Ramilison and Lienhard[22] indicated that the liquid-solid contact temperature at the onset of film boiling could be as high as the homogeneous nucleation temperature of the fluid if the advancing contact angle is high (approaching 180°). Although the contact angle of water on a clean copper surface was reported to be 90° by Liaw,[28] we nevertheless investigated the possibility of having the local point at the center of the dry patch be at the homogeneous nucleation temperature of the fluid as a bounding case. In doing this, we asked the following questions:

a) What dry patch area is necessary?
b) How quickly should the liquid macrolayer be evaporated in order to obtain the homogeneous nucleation temperature at the center of a dry patch?

To calculate the maximum possible dry patch area, an "infinitely large" copper heater with a radius of 300 mm was considered in the first calculation (Run 1). On the heater surface, the dry patch was assumed to appear instantly with a given size (the drying time of the liquid macrolayer in this region was assumed to be 0.0 ms). The heat-transfer coefficient, $h_2$, shown in Fig. 4, was used for the boundary condition on the wetted part of the heater. The dry patch radius required for the center temperature ($T_{TL}$) of the dry patch to exceed the homogeneous nucleation temperature of the liquid was calculated to be 44.4 mm. The other calculated parameters such as heater superheats at the four corners of the heater are listed in Table 1.

Table 1: Calculated STA Wall Heat Flux and Surface Temperatures

| Run No. | $t_d$ (ms) | $\delta_d$ ($\mu$) | $r_d/r_h$ | $r_d$ (mm) | $T_{av}$ (°C) | $q_{av}$ (MW/m$^2$) | $\Delta T_{BL}$ (°C) | $\Delta T_{BR}$ (°C) | $\Delta T_{TL}$ (°C) | $\Delta T_{TR}$ (°C) |
|---|---|---|---|---|---|---|---|---|---|---|
| 1 | 0.0 | 0.0 | 0.148 | 44.4 | 23.8 | 1.540 | 266 | 60.2 | 246 | 22.1 |
| 2 | 3.8 | 35.0 | 1.000 | 25.0 | 241 | 1.000 | 275 | 273 | 249 | 239 |
| 3 | 47.3 | 35.0 | 1.000 | 25.0 | 27.0 | 1.553 | 66.2 | 66.2 | 33.0 | 32.0 |
| 4 | 15 | 11.0 | 0.920 | 23.0 | 44.2 | 1.550 | 86.1 | 82.2 | 57.0 | 34.0 |
| 5 | 10.57 | 8.0 | 0.836 | 20.9 | 42.5 | 1.548 | 87.0 | 79.2 | 59.0 | 29.4 |
| 6 | 0.0 | 0.0 | 0.600 | 15.0 | 43.8 | 1.543 | 100 | 76.5 | 80.0 | 27.0 |
| 7 | 0.0 | 0.0 | 0.160 | 4.0 | 27.0 | 1.520 | 225 | 219 | 80.5 | 26.1 |
| 8 | 0.0 | 0.0 | 0.090 | 2.25 | 21.3 | 1.554 | 82.0 | 19.3 | 82.0 | 19.4 |

The calculated maximum dry patch radius (44.4 mm) is much larger than the heater size used by Gaertner (25.4 mm) and implies that the temperature at the center of dry patches at the occurrence of CHF in Gaertner's experiments must have been less than the homogeneous nucleation temperature of the liquid.

To answer the second question, a heater with a radius of 25 mm (the same size as Gaertner's heater) was considered. In this calculation (Run 2), we assumed that the whole heater surface was covered by the dry patch region (no macrolayer region existed). As a boundary condition on the heater surface, the heat-transfer coefficient $h_1$, obtained with an initial macrolayer thickness of 35 microns, was used. The drying time and its corresponding $h_1$ were varied until the temperature at the center of the

heater exceeded the homogeneous nucleation temperature of the water. The necessary drying time was found to be 3.8 ms (a fraction of the wet time, 81.3 ms), indicating almost instantaneous occurrence of the dry patch over the whole heater surface. The calculated wall superheats at the four corners of the heater and STA wall heat flux are listed in Table 1.

The above analysis indicates that the liquid-solid contact temperature at the occurrence of CHF should be well below the homogeneous nucleation temperature of the water in order to predict Gaertner's CHF data obtained on a thick copper heater with a radius of 25 mm. The requirement of relatively lower temperatures for liquid-solid contact to occur will result in relatively smaller dry patch sizes, as discussed below. The analysis also shows the importance of knowing when the dry patches occur.

**B. The Thickness of the Initial Macrolayer in the Dry Region of the Heater**

In section III.B, the upper bound of the initial macrolayer thickness in the dry patch region of the heater was estimated to be 35 microns. This number was calculated at the beginning of the second transition region. Below, we investigate whether the 35-micron macrolayer thickness is reasonable as an upper bound.

Using $h_1$ calculated for the initial macrolayer thickness of 35 microns in the dry patch region and $h_2$ for the macrolayer region, the size of the dry patch was varied to match the measured STA wall superheat at a CHF of 1.554 MW/m$^2$ in Run 3. The calculated STA wall superheats and heat fluxes with other parameters are listed in Table 1.

Even though the dry patch radius was selected to be 25 mm, the heat-transfer coefficient used in the dry patch region, $h_1$, and the drying time, $t_d$, were high enough to keep calculated STA wall superheat, 27 °C, less than measured value, 43°C. This again reflects the effectiveness of the latent heat in thin liquid layers to cool a surface, and implies that either a larger dry patch size or thinner liquid is needed to match the measured STA wall temperature.

Next, the initial thickness suggested by Haramura,[26] 11 microns, was assumed to exist prior to dry patch occurrence. It should be remembered that Haramura considers the surface-area-averaged initial macrolayer thickness. In our model, we specify a thickness for local macrolayers in the dry patch region. In Run 4, using $h_2$ and $h_1$ calculated with a initial thickness of 11 microns, a dry patch radius of 23 mm was found to be necessary to obtain a reasonable comparison between the calculated STA wall superheat and the measured value. The calculated STA wall heat flux and superheat for Run 4 are given in Table 1. The calculated and measured STA wall heat fluxes and temperatures are in good agreement. The radius of the dry patch is 23 mm (92% of the heater radius). Although Gaertner did not report any information on the size of the dry patch, from his sketch, the radius of the dry patch is expected to be less than 23 mm. In light of this information, the initial thickness of 11 microns could only be an upper limit. Thus, we conclude that more realistic bounds on the initial thickness of the macrolayer at the locations where the dry patches occur would be between 0 and 11 microns.

## C. The Critical Temperature for Liquid-Solid Contact at the Onset of the First Boiling Crisis

Above, we estimated a possible upper bound for the macrolayer thickness in the dry patch region. Using this maximum value, the wall surface temperature at the center of the dry patch ($T_{TL}$) was calculated to be 157°C at the end of the converged hovering period. This local-instantaneous temperature was considered to be the critical liquid-solid contact temperature for CHF to occur, because the calculation used an input heat flux that was observed as CHF in Gaertner's experiments. However, 157°C represents a lower bound for the critical liquid-solid (rewetting) contact temperature because it was calculated using a maximum possible macrolayer thickness. Based upon Gaertner's observation, the dry patch radius is expected to be smaller than 23 mm. This is only possible if a much smaller initial macrolayer thickness and, correspondingly, a shorter drying time were used for the dry patch region of the heater. Of course, one can expect that the critical rewetting temperature might increase with decreasing dry patch lifetime.

In this subsection, using Gaertner's CHF data, we will look for a possible range for the rewetting temperatures (superheats) at which no liquid-solid contact can occur. Therefore, two additional cases were considered as follows:

a) The dry patch was assumed to occur instantaneously (drying time was zero, implying that no heat transfer occurred in the dry patch region).

b) An initial thickness of 8 microns existed in the liquid macrolayer.

For these two cases, the calculated STA wall superheats were matched with the measured superheat by varying the size of the dry patch at the CHF point.

The results obtained for a $\delta_d$ of 8 microns in Run 5 are summarized in Table 1; the radial wall superheats are plotted as function of the heater radius in Fig. 5. When the $\delta_d$ (and thus the drying time, $t_d$) was decreased, the predicted dry patch radius decreased to 20.9 mm (83.6% of the heater radius), indicated by a vertical line in the figure. The calculated radial wall superheat profiles at the end of the hovering period at six different axial elevations are shown in Fig. 5. The number of hovering periods required for this run was 100. The instantaneous surface temperatures at the top the heater are fairly constant up to the heater radius of 20 mm. Then it gradually decreases to typical values calculated for the macrolayer region. The variations in temperature at the bottom of the heater are relatively small, about 2°C. The radial temperature profile a few millimeters beneath the surface becomes practically flat. The calculated wall superheat at the center of the dry patch increased to 59 °C.

The results for an $\delta_d$ of zero, Run 6, are given in Fig. 6, and the calculated STA wall heat flux and superheat are listed in Table 1. As shown in Fig. 6, the radial temperature profile becomes much steeper since no heat transfer was assumed to occur at the dry patch. The surface superheats in the macrolayer region are further decreased to about 27°C. The superheat at the center of the dry patch for this case is calculated as 80°C. The predicted radius of the dry patch becomes 15 mm (60% of the heater radius) as indicated in Fig. 6.

A quick summary of our results shows that the initial thickness of liquid macrolayers causing dry patch formation should vary between 0 and 11 microns. We found that the corresponding dry patch radii resulting from these thicknesses were 15 and 23 mm,

respectively. Our judgment, based upon the Gaertner's dry patch description, is that the dry patch radius of 23 mm is too large. Therefore, 11 microns is too thick. Consideration of an arbitrary 8-micron thickness yields a dry patch radius of 20.9 mm. Thus, we believe the initial dry patch macrolayer thickness varies between 0 and 8 microns. The calculated wall superheats at the center of the dry patch (local-instantaneous temperature) at which liquid-solid contact is no longer possible are 80°C and 59°C for macrolayer thicknesses of 0 and 8 microns, respectively.

Are these calculated rewetting temperatures realistic or reasonable? Unfortunately, we do not have experimental data to support the findings of the analysis we discussed above. However, Ramilison and Lienhard,[22] reported some limited information for contact temperature data at the onset of the transition-film boiling region as a function of contact angle. Their data is shown in Fig. 7 with the solid circles and rectangles. Figure 7 shows the fraction of the limiting liquid superheat at which the first contact occurs as a function of the advancing contact angle. The limit of the contact temperature as the advancing contact angle approaches zero (perfectly wetting fluid) is the homogeneous nucleation temperature of the liquid. An increase in the contact angle makes liquid-solid contact more difficult.

Liaw[28] reported that the contact angle was measured to be 90° for water on a clean copper surface. In Gaertner's study, the surface was cleaned before each test; thus, it is reasonable to assume that the contact angle in Gaertner's study was about 90°. Liaw and Dhir[29] also indicated that the contact angle of water on copper surfaces falls below the value of 90° if the heater surface oxidizes. In Gaertner's nucleate boiling experiments, the water was degassed; however, it is still possible that some air could have remained in the water, resulting in the oxidation of the copper surface during the experiments. In light of this statement and Liaw and Dhir's experimental observation,

the contact angle of water in Gaertner's experiments could have uncertainties as high as 50%, varying between 50° and 90°. In fact, for industrial applications, the contact angle of water is generally assumed to vary between 50° and 90°. Therefore, in Fig. 7, we indicate a contact angle of 90°, with an uncertainty band of –50%.

In Fig. 7, our calculated rewetting temperatures are compared with Ramilison and Lienhard's data and are indicated at a 90° contact angle point. It should be remembered that the local-instantaneous temperature at the center of the dry patch was relatively high, indicating that the surface was dry at the end of a hovering period. Thus, the liquid-solid contact at the beginning of the following hovering period can be characterized by the advancing contact angle. The calculated liquid-solid contact temperatures at the CHF do agree with the contact temperature at the onset of the liquid-solid contact in film boiling, if the Ramilison and Lienhard data is extrapolated by the line numbered with 1. If the calculated contact temperatures were plotted on their extrapolated curve (curve 2), the contact angle of water is estimated to vary between 60° and 70° (points A and B in Fig. 7). These values are in the expected range of the contact angle of water as discussed above. This indicates that the calculated contact temperatures at the onset of CHF are in good agreement with extrapolated contact temperatures at the onset of film boiling. Thus, the hypothesis we propose for the controlling mechanism of the CHF—that the local-instantaneous temperature at the center of a dry patch reaches a point where rewetting of the surface is no longer possible, causing a runaway condition—seems quite reasonable.

## D. The Effect of the Thermal Conductivity and Thickness of the Heater on Dry Patch Size

Several researchers have reported that the thermo-physical properties and the thickness of the heating surface may affect the boiling heat-transfer coefficient. A good summary of these studies is given by Pasamehmetoglu.[30] In most of the boiling tests that used either a thin heater or a nonisothermal material such as nickel, a second transition region did not exist and the results showed a sharp decrease in wall heat flux after the CHF. Because of these experimental observations, we investigate below the effect of the thermal conductivity and heater thickness on dry patch behavior.

To investigate the effect of thermal conductivity, a nickel heater with the same dimensions as the copper heater studied earlier (10 mm thick and 25 mm in diameter) was selected for Run 7. It was assumed that a dry patch with a given size occurs instantaneously ($t_d$ = 0 s). The dry patch radius necessary to obtain the same contact temperature at the center of the dry patch as the value calculated for the copper heater was found to be 4 mm (16% of the heater radius). The STA wall heat flux and superheat are listed in Table 1.

It is clear that the dry patch is much smaller for the nickel heater than the copper heater. It would be difficult to visually detect patches this small in experimental studies, and their effect on the boiling curve to create a second transition region should be minimal. For nonisothermal materials, the heat transfer becomes conduction controlled and the local-instantaneous wall temperature at the center of the relatively small dry patch reaches the critical rewetting temperature in relatively short times, leading to CHF at relatively lower heat fluxes.

To investigate the thickness effect, a calculation was performed for a copper heater with a thickness of 0.1 mm and with no heat transfer on the dry patch region (Run 8). A dry patch radius of 2.25 mm (9% of the heater radius) was enough for the temperature at the center of the dry patch to reach the rewetting temperature of 80°C. Dry patches with radii of 1 - 2 mm have been observed by Kirby and Westwater and Van Ouwerkerk, although their heater thicknesses were much smaller than 0.1 mm. In our calculation, further decreases in heater thickness would result in dry patch sizes smaller than 2.25 mm. Here, we only intend to demonstrate the importance of the heater thickness in determining the dry patch size. The other calculated parameters are given in Table 1. As it was in the case of a nonisothermal heater material, we believe the nucleate boiling curve would not indicate a second transition region if the heater is very thin.

The results obtained above for nonisothermal and thin materials did not require that the calculations be performed over several hovering periods and were obtained in a single hovering period. This indicates that the stationary dry patch assumption is not necessary. Thus, as observed by Van Ouwerkerk and Kirby and Westwater, the location of small dry patches varied for each hovering period.

## V. Summary and Conclusions

The model currently employed to study the boiling phenomenon in the second transition region of saturated pool nucleate boiling on a horizontal surface is a two-dimensional, transient-conduction model representing the heater and its boiling surface. The wetted portion of the heater, denoted as having a time-dependent, surface-averaged heat-transfer coefficient $h_2$, is characterized by a macrolayer having numerous vapor stems. The heat-transfer coefficient $h_2$ was obtained from the model

developed by Pasamehmetoglu and Nelson. Another time-dependent, surface-averaged heat-transfer coefficient, $h_1$, describes the dry patch behavior, which is related to the macrolayer initial thickness.

The current model assumes that the formation of dry patches is due to the evaporation of the local liquid macrolayers. Evaporation in the macrolayer only occurs in the axial direction, so that while the stem diameters do not change, the thickness of the liquid macrolayer decreases as a function of time. The thickness of the liquid macrolayer is assumed to vary from one point to another on the heater surface, showing some statistical distribution. The thinner macrolayer regions dry out first, forming dry patches. The model considers a dry patch with a given size to have a circular shape. No radial growth of the dry patch is considered. For thick copper heaters such as used by Gaertner, the dry patch had to be stationary for repeated hovering periods. For nonisothermal and thin heaters, however, dry patches could grow within a single vapor mushroom lifetime, so the stationary dry patch assumption was not required.

Utilizing the information provided by Gaertner, the initial macrolayer thickness on the dry portion of the heater was found to be bounded between 0 and 11 microns for a copper heater with infinite thickness. The corresponding dry patch radius varied from 15 to 23 mm, respectively. The liquid-solid contact temperature was found to vary from 179.8°C to 156.6°C for these bounding initial macrolayer thicknesses. These temperatures are much lower than the homogeneous nucleation temperature for water. The calculated contact temperatures were in good agreement with the extrapolated contact temperature data for the onset of film boiling.

We also found that the formation of the dry patch must occur over a number of hovering periods on a thick heater. The calculated minimum dry patch radius of 15

mm represents a significantly large area and has not been reported by any researchers either experimentally or analytically. Although it is possible that several dry patches of different sizes could occur on the surface, we think that, because the calculated dry patch size is high, the dry patch or patches on thick copper heater occur at a pseudo-stationary location. Therefore, the model considers a stationary dry patch.

To study the effects of thin heaters and heaters of different materials, we calculated the sizes of the dry patches associated with these changes. The radius of the dry patch for a nickel heater of the same size was small, 4 mm, using the same liquid-solid contact temperature obtained for the copper heater. When the thickness of the copper heater was decreased to 0.1 mm, the required dry patch radius was found to be 2.25 mm in order for the temperature at the center of the dry patch to reach the same critical contact temperature. This is believed to provide some explanation of why the second transition region has not been observed in these experimental situations. These results did not require the dry patch to be stationary and were thus obtained in a single vapor mushroom lifetime.

The occurrence of these patches alone is not sufficient to cause CHF. The temperature at the center of the dry patch must first reach a critical value above which liquid-solid contact is no longer possible. Once this condition occurs at a local point on the heater surface, the hot spot starts growing, causing the dry patch to finally cover the entire heater surface, as the surface moves through transition boiling into film boiling. We believe that the occurrence of such a hot spot on the surface is the real cause of the CHF. This hypothesis unifies the CHF with the quenching of hot surfaces by relating them both to the same governing mechanism, i.e., the ability of liquid to contact a hot surface.

The results obtained from the above analytical study are presented in the hope of furthering understanding of the mechanism governing the CHF. We envision future experiments which would investigate the dry patch characteristics implied for thick copper (i.e., pseudo-stationary, reasonably sized dry patches) to either discredit or further refine this hypothesis.

## VI. References


1) R. F. Gaertner, "Photographic Study of Nucleate Pool Boiling on a Horizontal Surface," *Journal of Heat Transfer* **15**, 401-428 (February 1965).

2) Y. Y. Hsu and R. W. Graham, *Transport Processes in Boiling and Two-phase Systems* (McGraw-Hill Book Company, 1976).

3) S. S. Kutateladze, "A Hydrodynamic Theory of Changes in Boiling Process Under Free Convection," *Izu. Akademia Nouk Otdelarie Tekh.* **4**, 529-536 (1951); AEC-TR-1441 (1954).

4) L. S. Sterman, "Theory of Heat Transfers in Boiling Liquids," *Zh. Tekh. Fiz.* **23**(2), 341-351, (1953); CTS-62 (1955).

5) V. M. Borishansky, "An Equation Generalizing Experimental Data on the Cessation of Bubble Boiling in Large Volume of Liquid," *Zh. Tekh. Fiz.* **26**(7), 452-456 (1965).

6) W. Rohsenow and P. Griffith, "Correlation of Maximum Heat Flux Data for Boiling of Saturated Liquid," *Chem. Engr. Prog. Symp. Ser.*, Vol. 52, No. 18 (1956).

7) Y. P. Chang and N. W. Snyder, "Heat Transfer in Saturated Boiling," *Chem. Engr. Prog. Symp. Ser.,* Vol. 56, No. 30, pp. 25-38 (1960).

8) Y. P. Chang, "A Theoretical Analysis of Heat Transfer in Natural Convection and in Boiling," *Trans. ASME* **79**, 1501-1513 (1957).

9) N. Zuber, "Stability of Boiling Heat Transfer," *Trans. ASME* **80**, 711-720 (1958).

10) N. Zuber, "Hydrodynamic Aspects of Boiling Heat Transfer," Ph.D. Thesis, University of California, Los Angeles (1959).

11) N. Zuber, M. Tribus, and J. W. Westwater, "The Hydrodynamic Crisis in Pool Boiling of Saturated and Subcooled Liquids," 2nd Int. Heat Transfer Conference, Denver, Colorado, 1961, paper 27.

12) D. B. Kirby and J. W. Westwater, "Bubble and Vapor Behavior on a Heated Horizontal Plate During Pool Boiling Near Burnout," *Chem. Engr. Prog. Symp. Ser.*, Vol. 61, No. 57 (1965).

13) C. L. Yu and R. B. Mesler, "Study of Nucleate Boiling Near the Peak Heat Flux Through Measurements of Transient Surface Temperature," *Int. J. Heat Mass Transfer* **20**, 827-840 (1977).

14) Y. Haramura and Y. Katto, "A New Hydrodynamic Model of Critical Heat Flux, Applicable Widely to Both Pool and Forced Convection Boiling on Submerged Bodies in Saturated Liquids," *Int. J. Heat Mass Transfer* **26**(3), 389-399 (1983).

15) K. O. Pasamehmetoglu and F. S. Gunnerson, "A Theoretical Prediction of the Critical Heat Flux During Power Transient; Part I: Saturated Pool Boiling," (to be published in *J. Heat Transfer*).

16) H. J. Van Ouwerkerk, "Burnout in Pool Boiling the Stability of Boiling Mechanism," *Int. J. Mass Heat Transfer* **15**, 25-34 (1972).

17) C. Corty and A. S. Foust, "Surface Variables in Nucleate Boiling," *Chem. Engr. Prog. Symp. Ser.*, Vol. 51, No. 17, pp. 1-12 (1955).

18) M. Carne, "Some Effects of Test Section Geometry in Saturated Pool Boiling on the Critical Heat Flux for Some Organic Liquids and Liquid Mixtures," *Chem. Engr. Prog. Symp. Ser.*, Vol. 61, No. 59, p. 281 (1965).

19) K. Torikai and T. Yamazaki, "Dry State in a Contact Area of a Boiling Bubble on a Heating Surface," *Bulletin of JSME* **10**(38) 1967.

20) R. A. Nelson, "Mechanisms of Quenching Surfaces," in *Handbook of Heat and Mass Transfer*, N. P. Cheremisinoff, Ed. (Gulf Publishing Company, Houston, Texas, 1986), Vol. 1, Chap. 35, pp. 1103-1153.

21) R. A. Nelson, "Quenching Mechanisms," chapter in *Post-CHF Heat Transfer*, (Hemisphere Publishing, in press).

22) J. M. Ramilison and J. H. Lienhard, "Transition Boiling Heat Transfer and Film Transition Regime," *Journal of Heat Transfer* **109**, 746-752 (August 1987).

23) C. Unal, V. Daw, and R. A. Nelson, "Unifying the Controlling Mechanism for the Critical Heat Flux: The Ability of Liquid to Contact the Hot Surface" (to be published as a Los Alamos National Laboratory document).

24) R. F. Gaertner and J. W. Westwater, "Population of Active Sites in Nucleate Boiling Heat Transfer," *Chem. Engr. Prog. Symp. Ser.*, Vol. 56, No. 30, p. 39-48 (1960).

25) K. O. Pasamehmetoglu and R. A. Nelson, "Pool Boiling Mechanisms in Saturated Liquids at High Heat Fluxes Near Critical Heat Flux" (to be published as a Los Alamos National Laboratory document).

26) Y. Haramura, "Characteristics of Pool Boiling Heat Transfer in the Vicinity of the Critical Heat Flux (Relations Between Bubble Motion and Heat Flux Fluctuations)," *Journal of the JSME* **53**, 490 (1987-6); (translated by Scripta Technica, 1989).

27) J. H. Lienhard, "Corresponding States Correlations for the Spinodal and Homogeneous Nucleation Temperature," *ASME Journal of Heat Transfer* **104**(23), 379-381 (1982).

28) S. P. Liaw, "Experimental and Analytical Study of Nucleate and Transition Boiling on Vertical Surfaces," Ph.D. thesis, Mechanical Engineering Department, University of California, Los Angeles (1988).

29) S. P. Liaw and V. K. Dhir, "Void Fraction Measurements During Saturated Pool Boiling of Water on Partially Wetted Vertical Surfaces," *Journal of Heat Transfer* **111**, 731-738 (August 1989).

30) K. O. Pasamehmetoglu, "Study of Heater Effects on the Nucleate Boiling Curve in Saturated Pool Boiling" (to be published as a Los Alamos National Laboratory document).

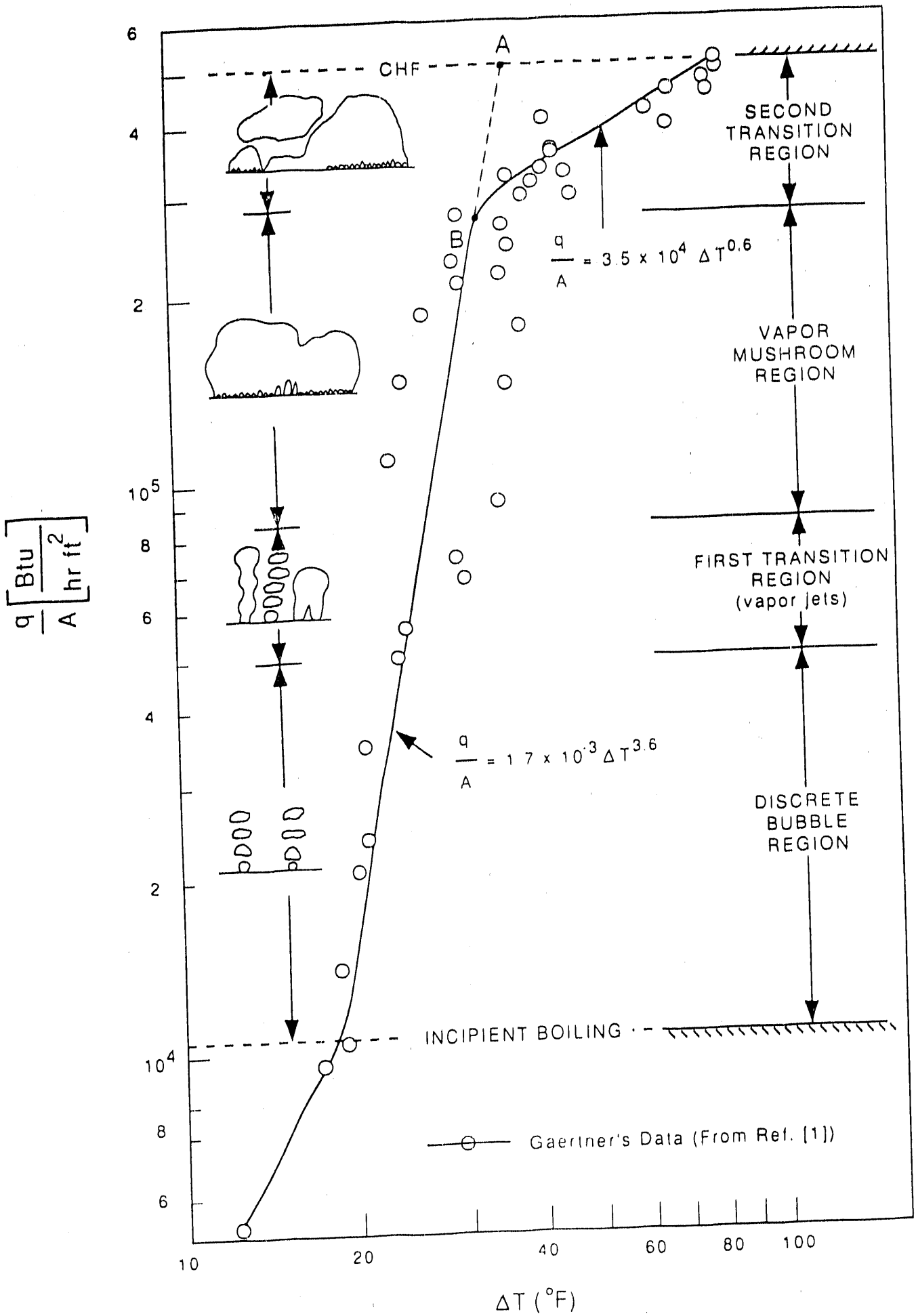


Figure 1: Gaertner's heat transfer data for water boiling on a polished thick flat horizontal copper plate.

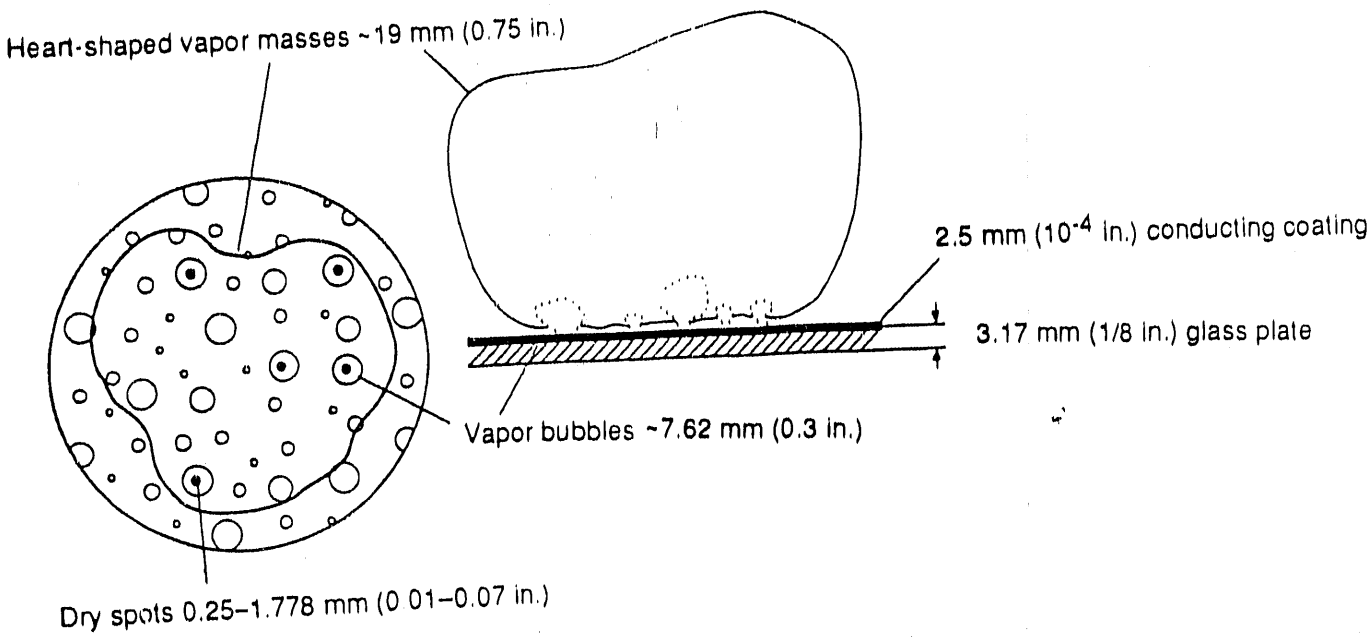


Figure 2-a: Sketch of vapor structure and dry spots observed by Kirby and Westwater (Ref. 12) on a flat horizontal thin plate.

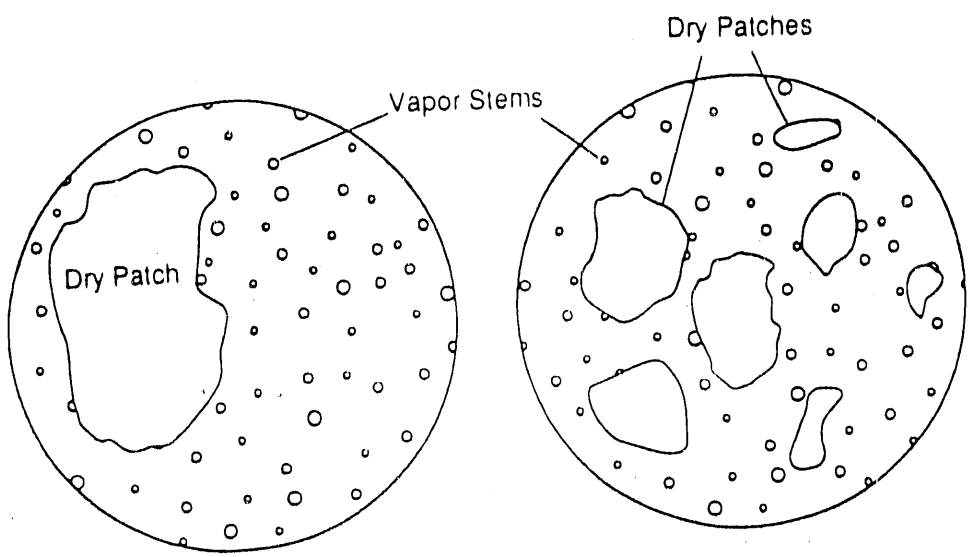


Figure 2-b: Sketch of imagined the top view of vapor structure and vapor patches in the second transition region.

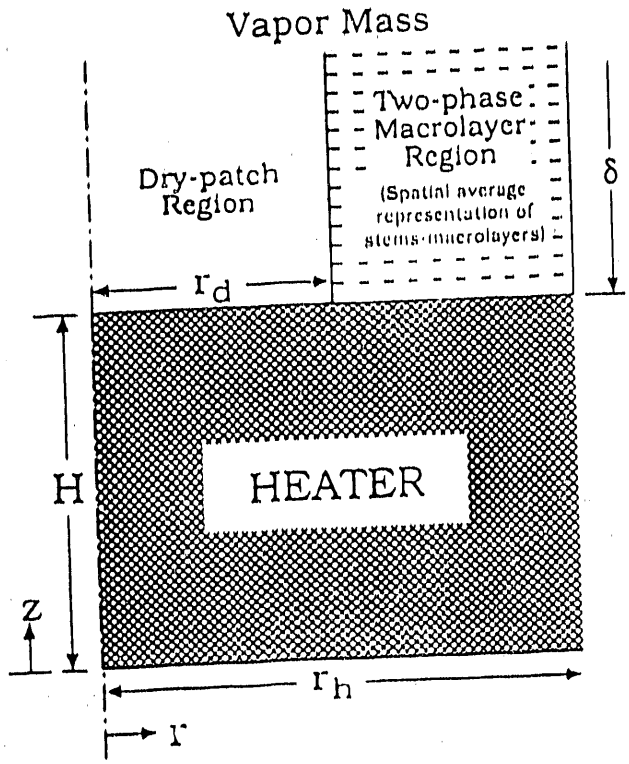


Figure 3-a: Sketch of the proposed heat transfer model for the second transition region of the nucleate boiling.

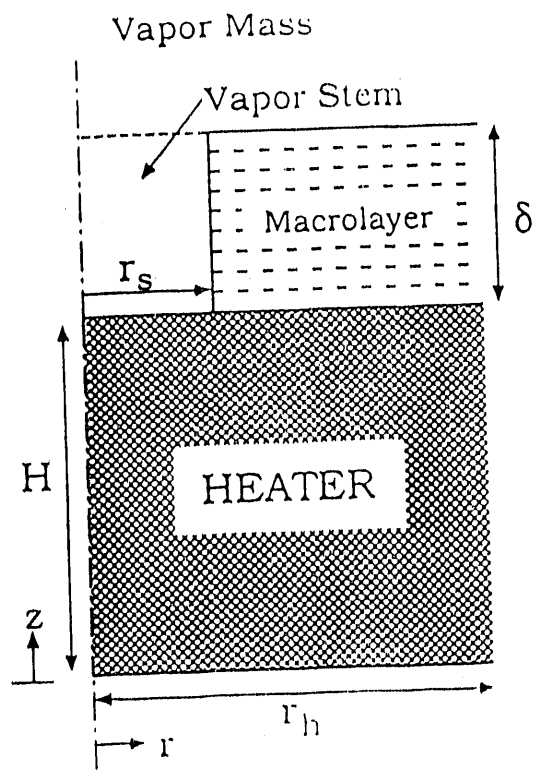


Figure 3-b: Sketch of heat transfer model (stem-macrolayer model) for pool boiling at high heat fluxes developed by Pasamehmetoglu and Nelson.

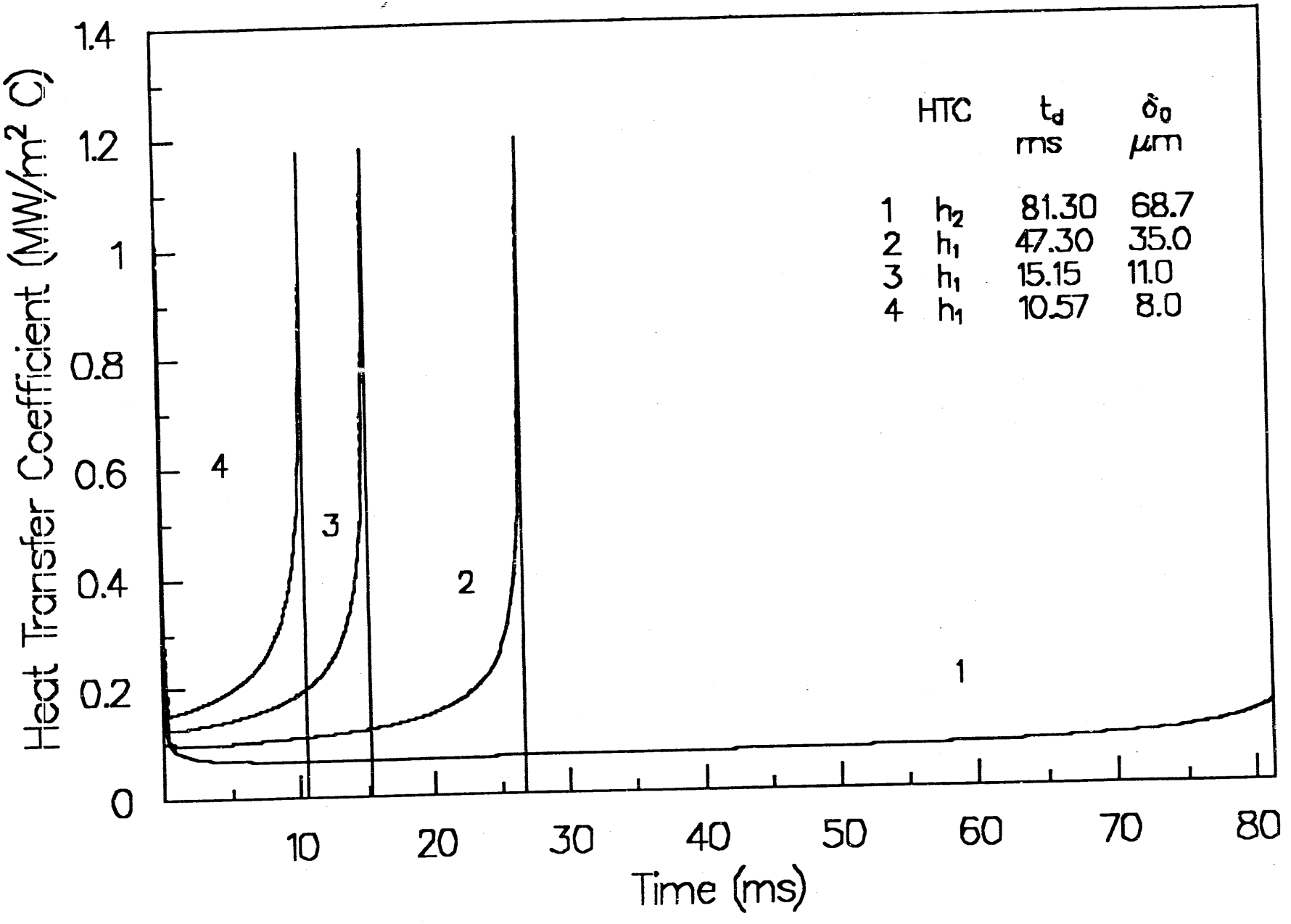


Figure 4: Instantaneous surface-averaged heat transfer coefficient representing dry patch and two-phase macrolayer regions for 10-mm-thick copper plate.

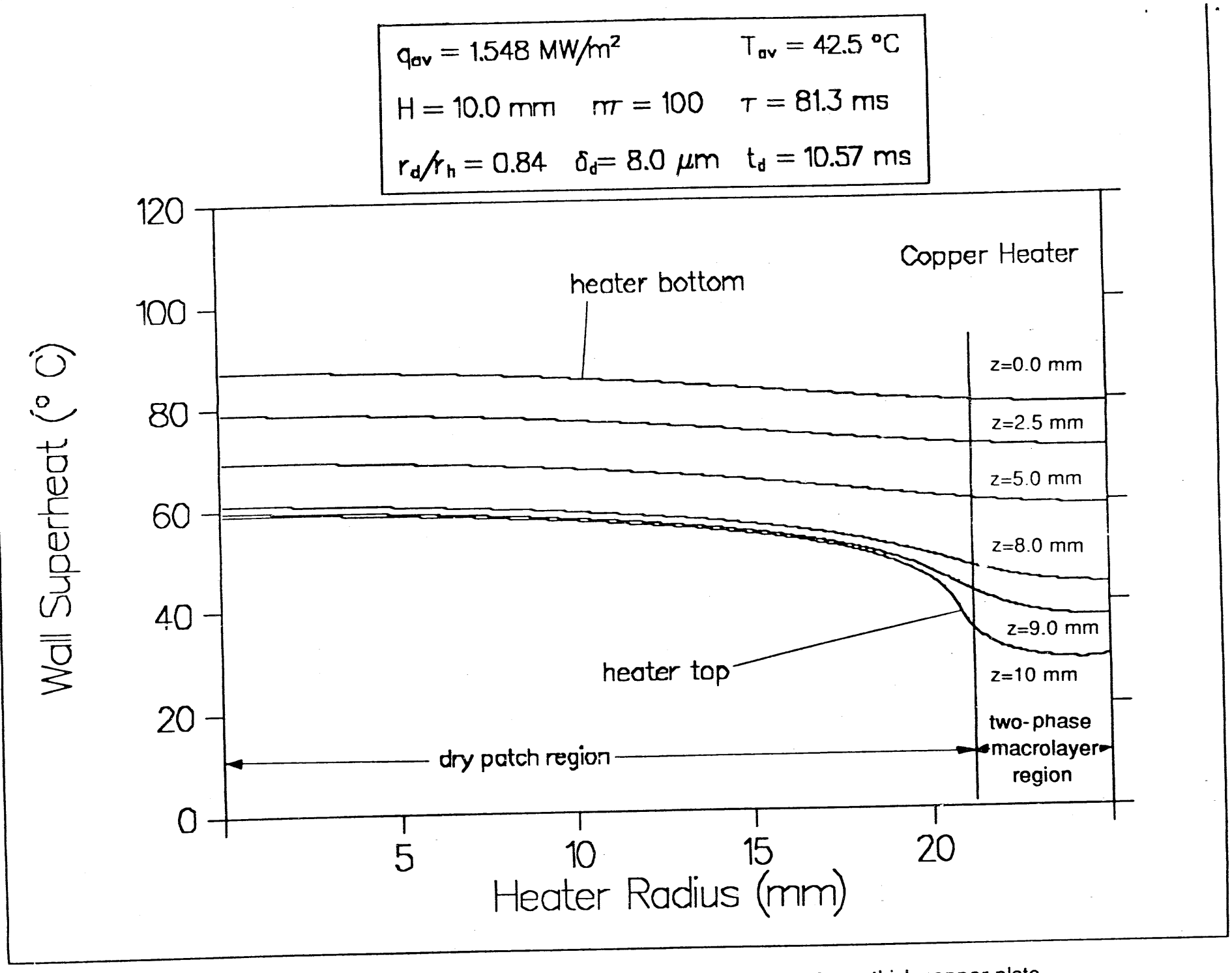


Figure 5: Calculated heater temperature distribution for 10-mm-thick copper plate using a heat transfer coefficient in the dry patch region that is obtained with a initial thickness of 8 micron.

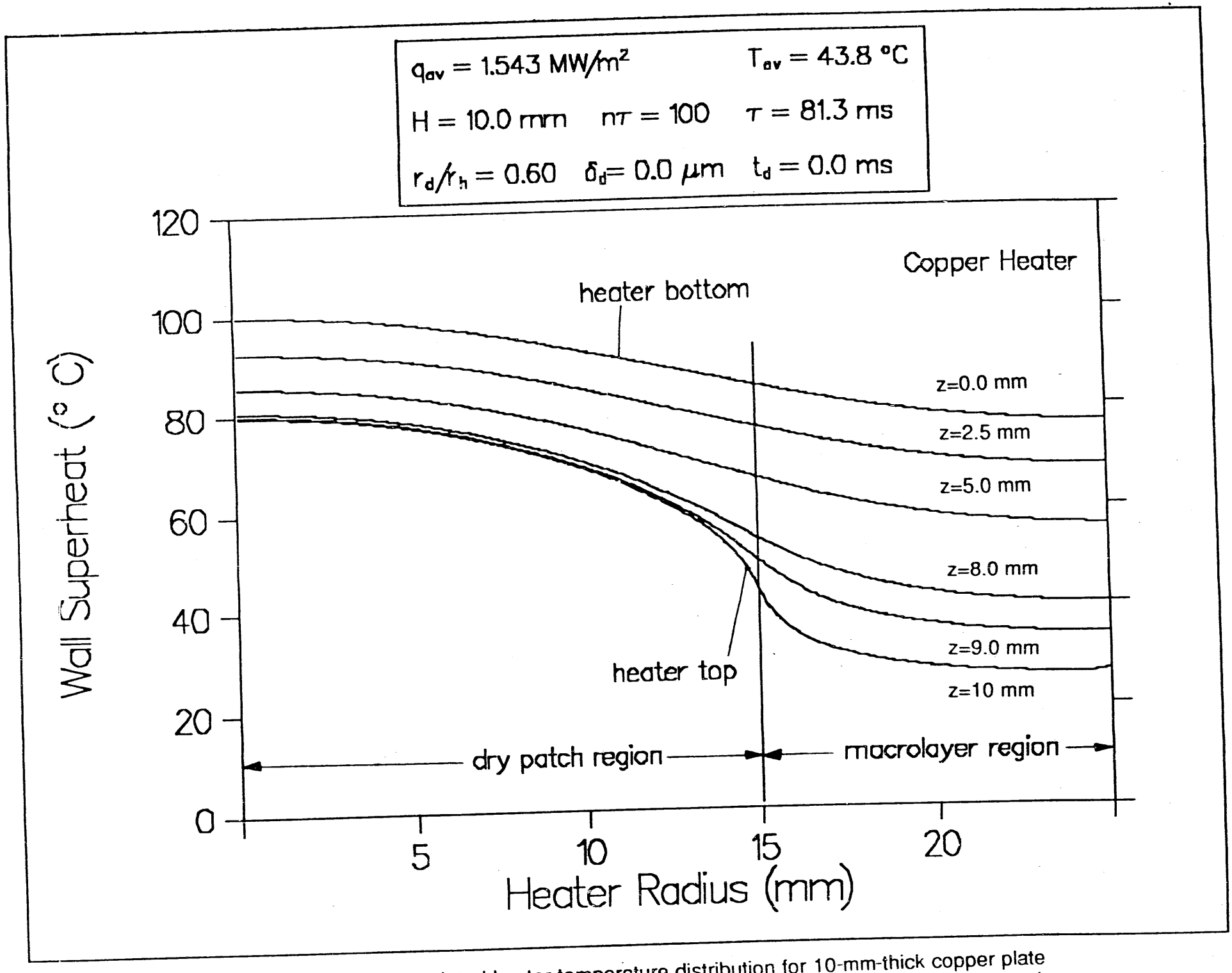


Figure 6: Calculated heater temperature distribution for 10-mm-thick copper plate using a heat transfer coefficient in the dry patch region that is obtained with a initial thickness of zero micron.

| | $\delta_d$ (micron) | $t_d$ (ms) | $r_d/r_h$ | $T_{av}$ (°C) | $q_{av}$ (MW/m$^2$) | $T_{rew}$ (°C) |
|---|---|---|---|---|---|---|
| △ | 0 | 0 | 0.60 | 43.8 | 1.543 | 79.8 |
| □ | 8 | 10.57 | 0.836 | 42.5 | 1.548 | 58.9 |
| ○ | 11 | 15.15 | 0.92 | 44.2 | 1.55 | 56.6 |
| ● | Ramilison and Leinhard Ref. [22] | | | | | |
| ■ | Berenson Ref. [22] | | | | | |

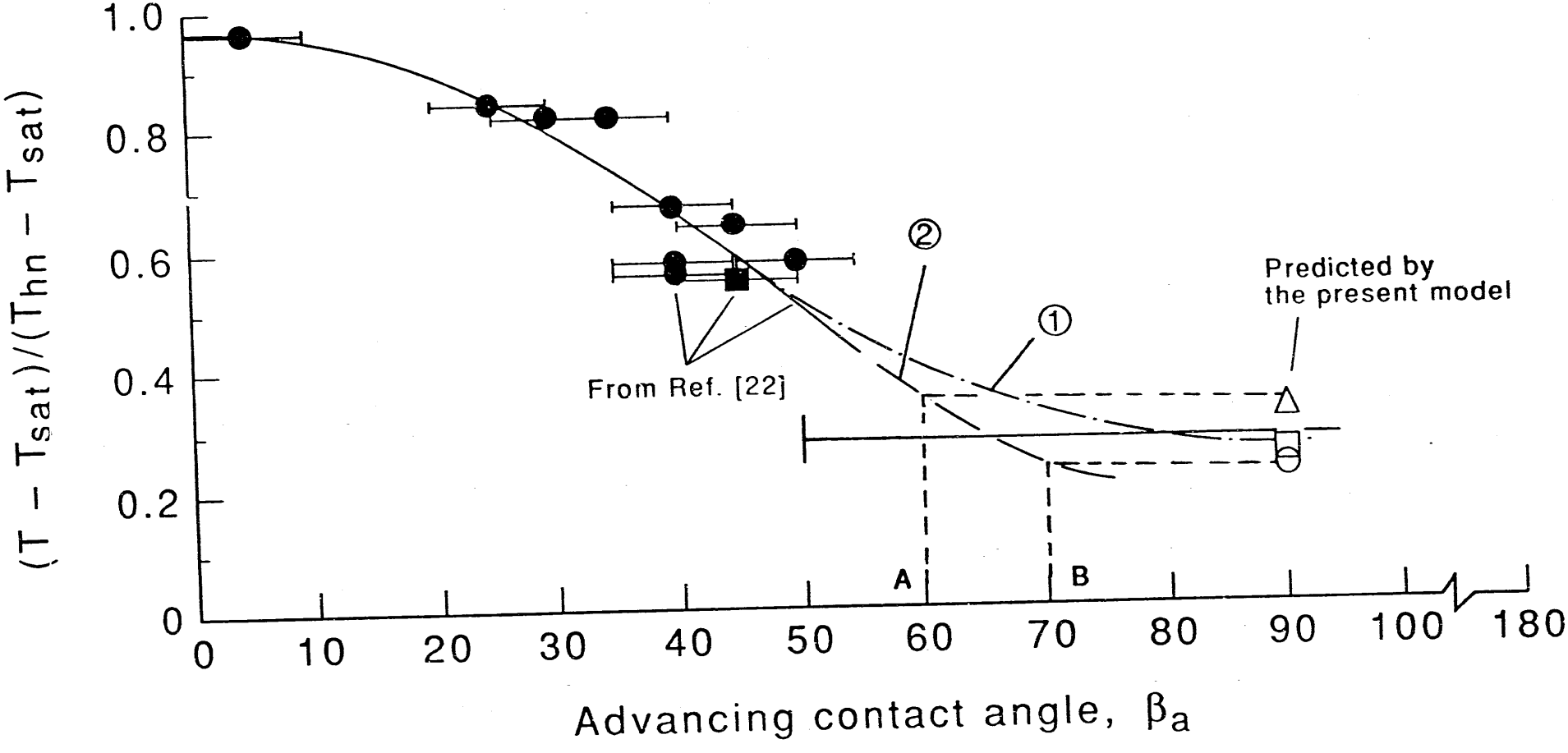


Figure 7: Calculated liquid-solid contact (rewetting) temperature at the onset of CHF.

END

DATE FILMED

06/07/91